ANL/APS/LS-331

5/14/2012

Magnetic Field Analysis of Helical Undulators

S.H. Kim
Advanced Photon Source, Argonne National Laboratory
9700 S. Cass Ave., Argonne, IL 60439, USA

Abstract – The analytical expression of the on-axis field for an infinitely long helical undulator, derived in terms of undulator period length, uniform current density, inner radius and dimensions of the coils, was compared with numerical analyses of model undulators based on the Biot-Savart law. The two calculations agreed within 1×10^{-3}. The expression also showed that the on-axis field has the first harmonic only, and no higher harmonics exist, regardless of the coil dimensions. Calculations for 61-period models showed that the third and fifth harmonics were less than 2×10^{-7}. For a finite-length model the end fields were adjusted by reducing the currents in a discrete number of steps for the last two or four periods of both ends. It was also shown as a practical method that increasing the coil winding radius can be a substitute for reducing the coil current.

1. Introduction

A helical undulator consists of a double helix carrying currents I_1 and I_2 in opposite directions in each helix, with one helix shifted from the other by a half-period along the undulator axis. The transverse and axial fields on the axis of the undulator are given by:

$$B_0 = \frac{\mu_0(I_1+I_2)}{\lambda}\left[kr_0K_0(kr_0)+K_1(kr_0)\right], \text{ and} \tag{1}$$

$$B_z = (\mu_0/\lambda)(I_1-I_2), \tag{1a}$$

where μ_0 is the permeability in free space, $k=2\pi/\lambda$ with λ as the helical winding period along the undulator axis, and K_0 and K_1 are modified Bessel functions. Equation (1) assumes that the helical undulator is wound with a filamentary wire on radius r_0, which makes the current density in the wire infinite. Generally, a helical undulator operates with $I_1 = I_2$, and the axial field of Eq. (1a) cancels out.

The transverse fields Eq. (1) for a single helix have been calculated by Smythe [1]. For a typical solenoid coil with $\lambda/r_0 << 1$, the transverse field is generally negligible. Alferov and his coworkers, and Kincaid have analyzed properties of circularly polarized synchrotron radiation from a short-period helical undulator [2, 3]. Elias and Madey developed the first superconducting (SC) helical undulator for an early free-electron laser experiment [4]. More recently, the proposed International Linear Collider includes a SC helical undulator system as the recommended option for the production of the positron beams [5]. Blewett and Chasman, Park and his coworkers, and other authors have derived the field configurations of helical undulators without any specific coil dimensions [6-9]. Tominaka and his coworkers have derived vector potentials and helical multipole coefficients for a single helical conductor [10]. Fajans has investigated finite-length helical fields and end-field perturbations [11].

We have derived the on- and off-axis magnetic fields in terms of specific coil dimensions and uniform current density for an infinite-length model of a double helix [12], but the analytical results of the on-axis field were never rigorously verified with numerical analyses of model undulators based on the Biot-Savart law. In the following section, the previously derived expressions are briefly summarized. In Section 3, the analytical results are compared with numerical analyses. In Section 4, the magnetic fields for a finite-length model are analyzed after adjusting the currents of end coils, and the conclusion is summarized in Section 5. The Vector Fields Software Opera was used for all model calculations in this paper [13].

2. On-Axis Field for an Infinite-Length Undulator

Figure 1 illustrates a model of the helical undulator coil with r_0 as the coil inner radius, a and b as the coil dimensions in the axial and radial directions, respectively, and j as the uniform current density in the coil. In the cylindrical coordinates (r, ϕ, z) with the z-axis on $r = 0$, a helix follows the winding along $z = \phi/k$, and the periodic helical field on the z-axis may be expressed as:

$$\mathbf{B}(kz-\phi) = B_0\left\{\hat{r}\cos(kz-\phi) + \hat{\phi}\sin(kz-\phi)\right\}, \tag{2}$$

where $\hat{r}$ and $\hat{\phi}$ are unit vectors in the r and ϕ coordinates. When the winding direction is reversed, ϕ may be replaced with $-\phi$. Equation (2) may be converted into the Cartesian coordinates (x, y, z).

$$\mathbf{B} = B_0\left\{\hat{x}\cos(kz) + \hat{y}\sin(kz)\right\}. \tag{2a}$$

The current density J per unit thickness in the radial direction of an infinitely long double helix, as shown in Fig. 1, may be expressed as the following Fourier series in the cylindrical coordinates (r, ϕ, z):

$$J(kz-\phi) = \sum_{n=1}^{\infty}\frac{4j}{n\pi}\sin(\frac{n\pi}{2})\sin(nk\frac{a}{2})\sin n(kz-\phi), \tag{3}$$

where j is the current density per unit cross section of the double helix. The origin of the z-axis in Fig. 1 is chosen to be at the middle of a helix viewing from the top-to-bottom direction, y-axis, but Eq. (3) is based on the view from the x-axis. The scalar potentials, $\Phi_<$ for $r < r_0$, and $\Phi_>$ for $r > r_0$, must be finite, and must satisfy the boundary condition for the continuity of the field component normal to the radius at $r = r_0$. The two potentials in cylindrical coordinates have been calculated as [11]

$$\Phi_< = \sum_{n=1}^{\infty}\frac{4jr_0}{n\pi}\sin(\frac{n\pi}{2})K_n'(nkr_0)\sin\left(\frac{nka}{2}\right)I_n(nkr)\cos n(kz-\phi), \text{ and} \tag{4a}$$

$$\Phi_{>} = \sum_{n=1}^{\infty} \frac{4jr_0}{n\pi} \sin(\frac{n\pi}{2}) I_n^{'}(nkr_0) \sin\left(\frac{nka}{2}\right) K_n(nkr) \cos n(kz-\phi), \tag{4b}$$

where I_n and K_n are modified Bessel functions of the nth order, and the primes denote differentiations of the Bessel functions with respect to their arguments.

For $r < r_0$, the three field components were calculated from Eq. (4a) and $\mathbf{B}_{<} = -\mu_0 \nabla \Phi_{<}$ as

$$\mathbf{B}_{<} = \sum_{n=1}^{\infty} B_0^n \cdot \sin(\frac{n\pi}{2}) \left\{ \hat{r} \left[I_{n-1}(nkr) + I_{n+1}(nkr) \right] \cos n(kz-\phi) \right.$$
$$\left. + \hat{\phi} \left[\frac{2}{kr} I_n(nkr) \right] \sin n(kz-\phi) + \hat{z} \left[-2 I_n(nkr) \right] \sin n(kz-\phi) \right\}, \tag{5}$$

where

$$B_0^n = \frac{2\mu_0 j}{\pi} \sin\left(\frac{nka}{2}\right) \left[kr_0 K_{n-1}(nkr_0) + K_n(nkr_0) \right]. \tag{6}$$

Also, from the series expansion of $I_n(nkr)$ for $r \to 0$:

$$I_n(nkr) = \sum_{\ell=0}^{\infty} \frac{(nkr/2)^{n+2\ell}}{\ell!(n+\ell)!}, \tag{7}$$

the only non-vanishing terms on the z-axis in Eq. (5) are the first term for the radial field and the azimuthal field with $n = 1$. Then, Eq. (6) is reduced to

$$B_0^1 = \frac{2\mu_0 j}{\pi} \sin\left(\frac{ka}{2}\right) \left[kr_0 K_0(kr_0) + K_1(kr_0) \right], \tag{8}$$

which may replace the B_0 in Eqs. (2) and (2a) for the current density Eq. (3). The coil dimension in the radial direction may now be extended from r_0 to ($r_0 + b$), and the on-axis field B_0^1 may be expressed as the following:

$$B_0 = \frac{2\mu_0 j\lambda}{\pi} \sin(k\frac{a}{2}) \int_{r_0}^{r_0+b} \{ krK_0(kr) + K_1(kr) \} \frac{dr}{\lambda}. \tag{9}$$

The on-axis field B_0 does not depend on z-position, but B_0 is the peak field for the x- and y-components in Eq. (2a). It should be noted from Eq. (9) that, when undulator dimensions are scaled according to a period ratio, the on-axis field should be proportional to $j\lambda$. The field components for $r > (r_0 + b)$ may be calculated from Eq. (4b) and $\mathbf{B}_{>} = -\mu_0 \nabla \Phi_{>}$.

From Eq. (5) off-axis field components for $n = 1$ near the z-axis may be approximated, using Eq. (7):

$$B_r^1 = B_0 \left\{ 1 + \frac{3(kr)^2}{8} + \frac{5(kr)^4}{192} + \ldots \right\} \cos(kz-\phi),$$

$$B_{\phi}^{1} = B_0 \left\{ 1 + \frac{(kr)^2}{8} + \frac{(kr)^4}{192} + ... \right\} \sin(kz - \phi), \tag{10}$$

$$B_{z}^{1} = -B_0 \left\{ kr + \frac{(kr)^3}{8} + ... \right\} \sin(kz - \phi).$$

3. Comparison with Model Calculations

The on-axis fields B_0 were calculated from Eq. (9) for an undulator with parameters λ = 12, r_0 = 3.15, b = 4.0, a varied from 0.5 to 5.99 (*all in mm units*), and j = 1 kA/mm^2. Then, the data were compared with model calculations for the middle section of a 61-period helix, which used the software OPERA based on the Biot-Savart law [13]. The number of periods was chosen to be able to neglect the effect of the end field in the middle section of the undulator. The two sets of calculations are plotted in Fig. 2. Initially, there were large discrepancies between the analytical expression and numerical analyses, especially when the coil dimension a was chosen to be near $\lambda/2$. The discrepancies diminished only when the tolerance specifications of the numerical calculations were tightened [14]. Figure 3 shows that the two sets of the calculations in Fig. 2 agree within 1×10^{-3}, but it is not known why the OPERA calculations were systematically larger than the analytical results.

In order to look at higher harmonics of the on-axis field, the field component $B_y(z)$ of the 61-period model undulator was first calculated for one period in the middle section of the model and normalized to its peak field B_0. Then, after subtracting the first harmonic field $sin(kz)$ from the normalized field $B_y(z)/B_0$, the residuals were plotted in Fig. 4 (*top*). Similar calculations for $B_x(z)$ were plotted in Fig. 4 (*bottom*). Analysis showed that the 3rd and 5th harmonics of the residuals for the normalized fields, $sin(nkz)$ *and* $cos(nkz)$ with n = 3 and 5, were less than 2×10^{-7} for the selected four values of the coil dimension a.

As shown in the Appendix, the above results are different from those for a planar-type undulator. Depending on the coil dimensions, higher harmonics with a magnitude of a few percent are listed in Table 1. Other types of helical undulators, mostly permanent-magnet-based devices [15-17], have been built. But, in order to compare with the above results, the measured magnetic field data require considerable accuracy, and it must be known whether the devices, in principle, have higher harmonics or not. Analysis of measured data for a 20-period SC helical undulator showed that, excluding the end-field, higher harmonic coefficients up to the 5th harmonic were about 5×10^{-3} [18]. The larger harmonics, which are much larger compared to the analysis results shown in the next section, may be due to some errors in measurements and in fabrication.

4. Analysis of a Finite-Length Undulator

When the number of periods for the 61-period model gradually reduced down to 21 periods, the higher harmonics of the on-axis field started to increase. The 21-period model

may be considered as a finite-length undulator. In the middle (z = 0) the largest harmonic coefficient was about 6.5×10^{-6} and the relative on-axis field decrease was less than 5×10^{-5}. The harmonic coefficients increased as the position assumed for the calculation moved from the middle toward an end; 8×10^{-6} for the 3rd period, 3×10^{-5} for the 5th period, and 1.7×10^{-4} for the 7th period.

Since the factor $[krK_0(kr) + K_1(kr)]$ in Eq. (9) is approximately a form of $\exp(-skr)$ with s as a constant, reducing the current or current density is equivalent to increasing the winding radius as analyzed by Fajans [11] and Fig. 2 in [12]. Fajans analyzed the end field with two methods: flared the winding radius outward and "staggered terminations." The latter method uses "loop terminators" in every half period to reduce the coil current in discrete steps. Both methods have been analyzed by applying to six periods for one end, and the end fields have been reduced linearly from the nominal on-axis field to near zero. Recently, only a one-period correction coil for each end was used to tune the required end field for a SC planar undulator at the APS [19]. Also in [18], the end field was terminated within one period length in an experimental helical undulator, and conductors with current in the opposite directions were paired to minimize undesired fields.

Figure 5 is a plot to show that increasing the coil inner radius is equivalent to reducing the current density. The normalized on-axis fields were calculated from Eq. (9) with $\lambda = 12$, $a = 4.0$, $b = 3.84$, $r_0 = 3.15$, and $j = 1.0$. When the current density is reduced to 0.4, for example, the normalized field will be 0.4, which can also be obtained without reducing the current density but by increasing the inner radius to 5.0. Since the staggered terminations may be not practical for multi-turn coils, end-coil currents were artificially reduced as follows.

Two end-field models with 21 periods were adjusted by reducing the currents discretely for two periods and for four periods at each end of the model. The first model had 16 discrete steps of the current assignments as follows. First, as shown in Fig. 6(*a*), each coil length for the two periods was divided into 16 equal-length segments. Then, starting from the first segment at the end of a coil, 1/16 of the current was assigned to the first segment, 2/16 to the second, and so on until assigning the full current to the 16th segment.

The calculated field components B_y and B_x are plotted in Fig. 6(*b*) for the left half of the undulator. B_y and B_x are anti-symmetric and symmetric with respect to $z = 0$, respectively. This is due to the fact that the y-axis passes through in the middle of a coil while the x-axis passes through the "air pole" between two coils. Consequently, the first integral for B_y becomes null though the integral for the half side $z < 0$ was about -1.172 T-mm, and the first integral for the symmetrical B_x was about 0.0214 T-mm with one half of it from each side:

$$\begin{aligned} &\int_{-\infty}^{0} B_y(z)dz + \int_{0}^{\infty} B_y(z)dz = 0, \\ &\int_{-\infty}^{\infty} B_x(z)dz = 0.0214. \end{aligned} \tag{10}$$

The first and second integrals for B_y and B_x are plotted in Fig. 7. About 1.2 T-mm for the peaks of the first integrals is equivalent to about 50 μrad for the maximum electron beam angle with a beam energy of 7 GeV. Also, the second integrals of about 14.2 T-mm^2 for B_y and 8.2 T-mm^2 for B_x in Fig. 7 correspond to electron beam shifts of about 0.65 μm and 0.35 μm, respectively, for the same beam energy.

Also, starting from one end of a coil, the current of the first segment started with 1/32, instead of 1/16, of the full current for the first segment. The current was increased by 1/32 per segment. After increasing the current up to the 32nd segment of four periods, it reached the full current. Field components B_y and B_x are plotted in Fig. 8. The linearly decreasing end field is similar to a flared case in [11]. Compared with Fig. 7, the second integral plotted in Fig. 9 for B_y decreased by about 45%.

After rotating the undulator from the current reference position to an angle ϕ around the z-axis, as expected the new field components are calculated as

$$B_y(z,\phi) = B_y(z)\cos\phi - B_x(z)\sin\phi, \text{ and} \tag{11a}$$

$$B_x(z,\phi) = B_y(z)\sin\phi + B_x(z)\cos\phi, \tag{11b}$$

and the first field integrals for the second terms vanish. Therefore, at an arbitrary angle ϕ, the electron beam angle and the beam shift will not be much different from those shown in Fig. 7 and Fig. 9. Regardless of the above results, a finite-length helical undulator will require correction coils for B_y and B_x to adjust the field contributions from non-integer parts of windings and to compensate fabrication tolerances.

5. Conclusion

Analytical expressions of the magnetic field for an infinitely long helical undulator are summarized in terms of undulator period length, uniform current density in the coil, inner radius of the coil winding, and coil dimensions. The on-axis fields of the derived expression agreed with numerical calculations based on the Biot-Savart law for 61-period models to within 1×10^{-3} under tight tolerance specifications of the numerical calculations. Higher harmonics of the normalized fields, $[B_y(z)/B_0]sin(nkz)$ and $[B_x(z)/B_0]cos(nkz)$, analyzed for model calculations were less than 2×10^{-7}, confirming that the derived analytical expression has the first harmonic only. Higher harmonics for typical planar undulators are on the order of 10^{-2} as shown in the Appendix. The corresponding harmonics for a finite-length model (21 periods) were larger than 6.5×10^{-6} due to the end fields. It was shown that the end field may be adjusted by reducing the currents in discrete steps along the length for two or three periods of the coil ends. Reducing the current is not practical, but increasing the coil winding radius is a practical substitute.

Acknowledgments

The author is indebted to E.R. Moog for her critical reading of the manuscript and useful suggestions. This work was supported by the U.S. Department of Energy, Office of Science, under Contract No. DE-AC02-06CH11357.

Appendix

Generally for planar-type undulators, the vertical field along the beam axis in the undulator midplane contains higher harmonic contributions in addition to the fundamental one. As an example, the vertical field was calculated for a period of 12.0 mm, pole gap of 4.0 mm, coil dimension in the vertical direction of 3.5 mm, and three coil dimensions a in the beam direction. Plotted in Fig. 10 and Fig. 11 are the vertical field normalized to the corresponding peak field B_0 and the residual field after subtracting the fundamental field. As summarized in Table 1, third-harmonic coefficients were a few percent of the fundamental.

Table 1: Calculated B_0 and higher harmonics

	a = 1 mm	a = 3 mm	a =5 mm
B_0 (T)	0.2331	0.6368	0.8804
3rd (10^{-2})	-4.43	-1.62	1.19
5th (10^{-2})	0.27	-0.07	0.02

References

[1] W.R. Smythe, *Static and Dynamic Electricity* (McGraw-Hill, New York, 1939), p. 272.
[2] D.F. Alferov, Yu.A. Bashmakov, and E.G. Bessonov, Sov. Phys. Tech. Phys. 18 (1974) 1336; 21 (1976) 1408.
[3] B.M. Kincaid, J. Appl. Phys. 48 (1977) 2684.
[4] L.R. Elias and J.M. Madey, Rev. Sci. Instrum. 50 (1979) 1335.
[5] http://www.linearcollider.org/cms/
[6] J.P. Blewett and R. Chasman, J. Appl. Phys. 48 (1977) 2692.
[7] S.Y. Park, J.M. Baird, R.A. Smith, and J.L. Hirshfield, J. Appl. Phys. 53 (1982) 1320.
[8] I. Kimel, L.R. Elias, and G. Ramian, Nucl. Instrum. Methods A 250 (1986) 320.
[9] M. Calvo and O. Rendon, Rev. Sci. Instrum. 61 (1990) 124.
[10] T. Tominaka, Nucl. Instrum. Methods A 523 (2004) 1; T. Tominaka, M. Okakura, and T. Katayama, *ibid*. A 484 (2002) 36; *ibid*. A 459 (2001) 398.
[11] J. Fajans, J. Appl. Phys. 55 (1984) 43.
[12] S.H. Kim, Nucl. Instrum. Methods A 584 (2008) 266.
[13] Opera, Vector Fields Software, Cobham Technical Services, Aurora, IL 60505, USA.
[14] S.H. Kim, "Magnetic Field Calculation of a Helical Undulator: Analytical and OPERA Model with Tolerance Parameter," Third Special Workshop on Magnet Simulations for Particle Accelerators in PAC09, Vancouver, BC, Canada, May 5-6, 2009.
[15] K. Halbach, Nucl. Instrum. Methods 187 (1981) 105.
[16] S. Sasaki, Nucl. Instrum. Methods A 347 (1994) 83.
[17] T. Hara et al., Nucl. Instrum. Methods A 467-468 (2001) 165.
[18] S.H. Kim and C.L. Doose, "Development of a Model Superconducting Helical Undulator for the ILC Positron Source," Proc. 2007 PAC (2007) p. 1136, http://www.jacow.org.
[19] C.L. Doose, M. Kasa, S.H. Kim, "End-Field Analysis and Implementation of Correction Coils for a Short-Period NbTi Superconducting Undulator," Proc. 2011 PAC, p. 1180.

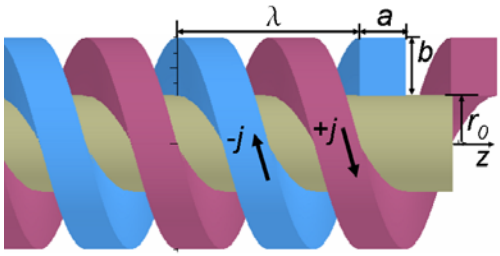

Fig. 1. A section of helical undulator model is depicted, with λ as the period length, r_0 as the inner radius of the coil, a and b as the coil dimensions in the beam and radial directions, respectively, and j as the current density in the double helix,

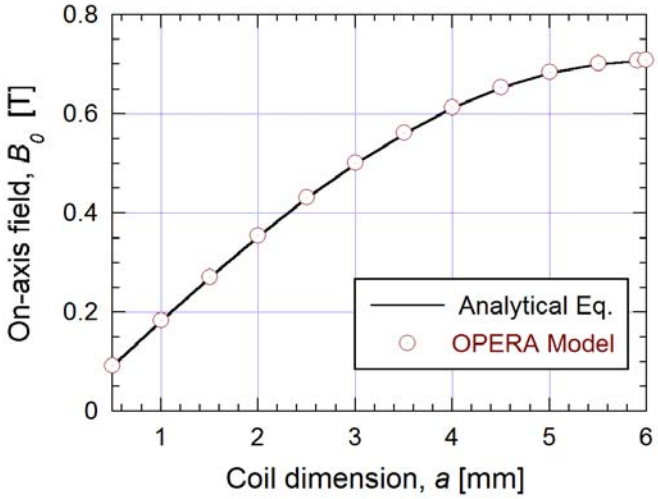

Fig. 2. The on-axis fields B_0 on the undulator axis calculated from Eq. (9) and Opera models are plotted for undulator parameters of period λ = 12, r_0 = 3.15, b = 3.84 (*all in mm units*), and j = 1 kA/mm^2. Coil dimensions a, shown in Fig. 1, were selected from 0.5 to 5.99.

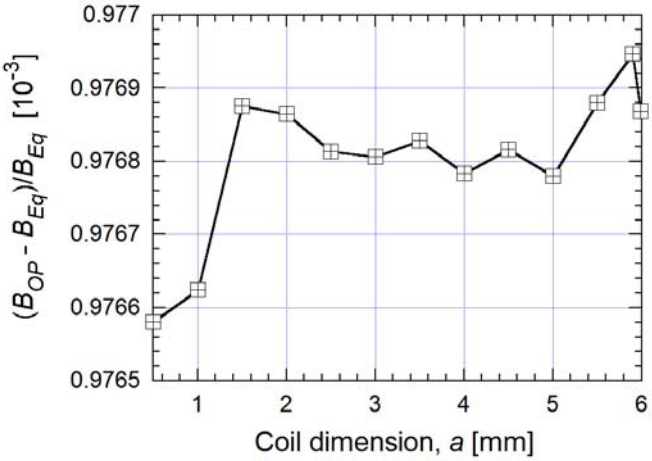

Fig. 3. The calculations of B_0 in Fig. 2 from Opera model B_{Op} and from Eq. (9) B_{Eq} are compared. The two calculations agree within 1×10^{-3}.

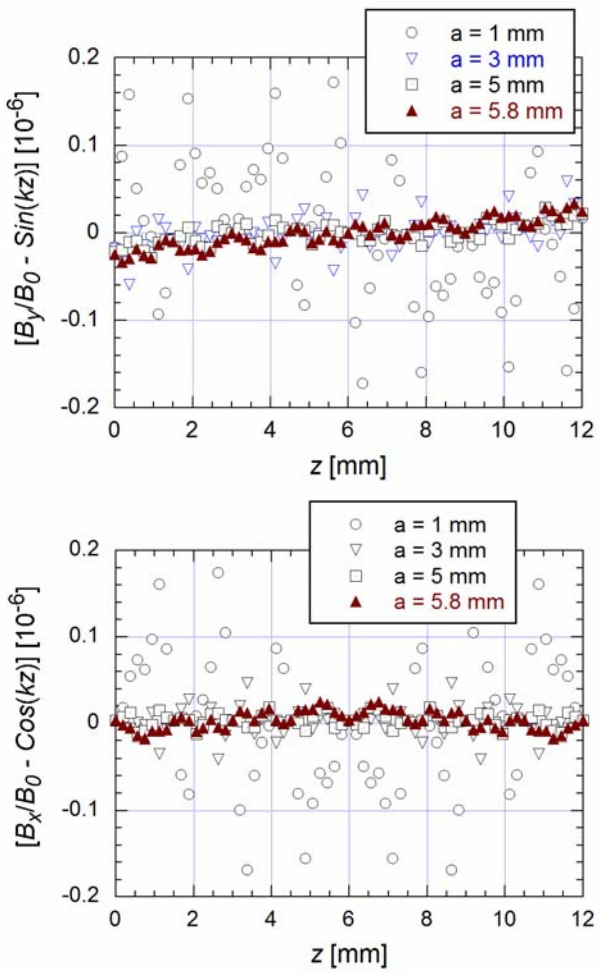

Fig. 4. Components of the on-axis fields, normalized to the corresponding on-axis field B_0, were plotted after subtracting the first harmonic field. The plots show that normalized residual fields for the selected four values of the coil dimension are less than 2×10^{-7} for both (*top*) $B_y(z)$ and (*bottom*) $B_x(z)$.

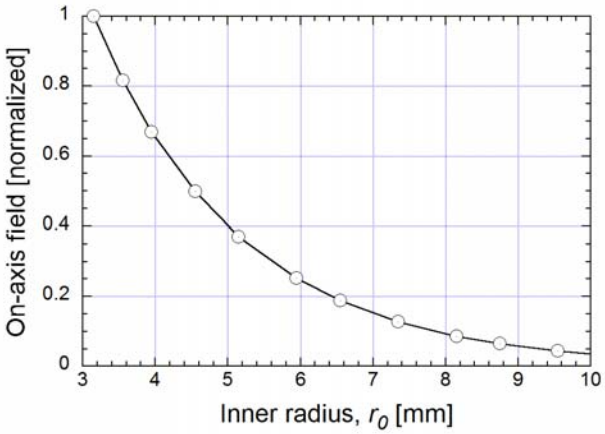

Fig. 5. On-axis fields, calculated from Eq. (9) with $\lambda = 12$, $a = 4.0$, $b = 3.84$ (*all in mm units*), and $j = 1.0$ kA/mm^2, are plotted for the inner radius from 3.15 to 9.65. The normalizing field at $r_0 = 3.15$ was 0.6126 T. The figure indicates that increasing the coil radius can be a substitute for reducing the coil current.

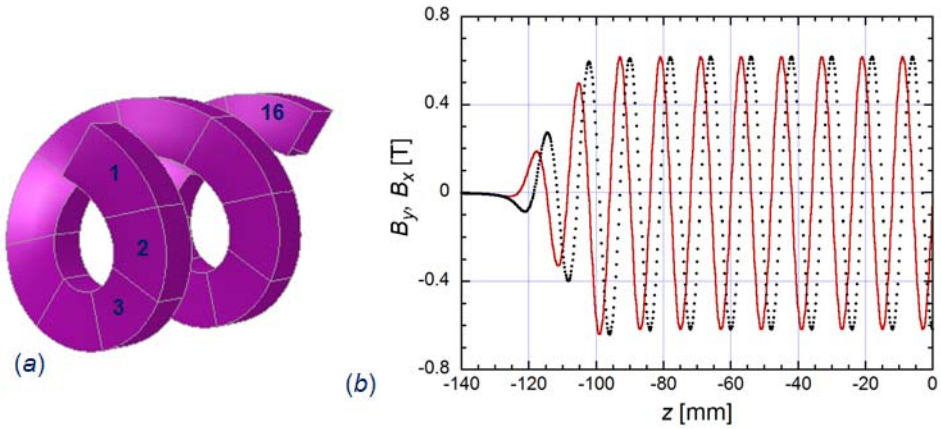

Fig. 6. (*a*): A two-period end coil was divided into 16 segments to increase the coil current discretely from 1/16 for the 1st segment to the full current for the 16th segment. (*b*): Field components for the left half of the undulator show the end-field variations after gradually reducing the coil currents for the end segments of *two periods*. The data represented as a *continuous line* are for B_y and those represented as *dots* are for B_x.

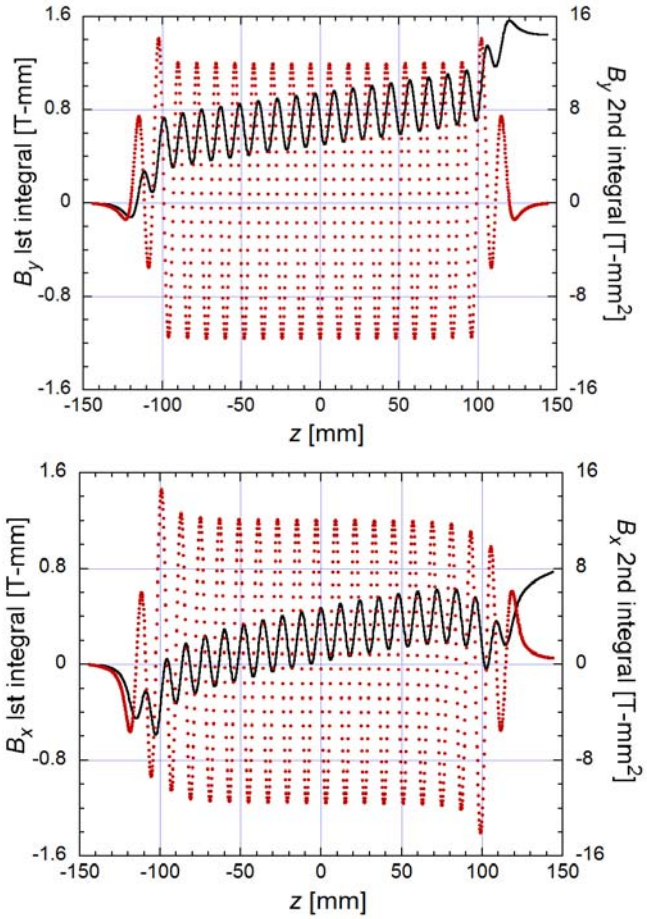

Fig. 7. Field integrals for B_y and B_x show the effect of end fields plotted in Fig. 6. The first integrals, represented as *dots*, are almost zero, and the second integrals for B_y and B_x, represented as *continuous lines*, are of about 14.5 T-mm^2 and 8.2 T-mm^2, respectively.

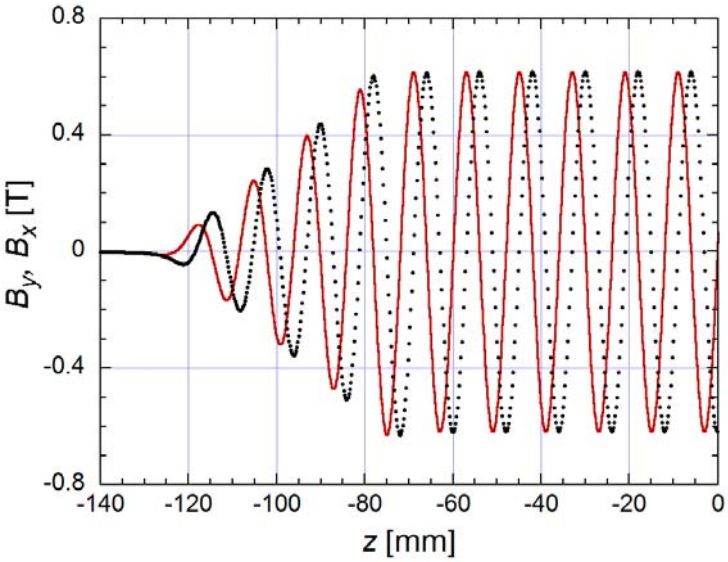

Fig. 8. With the same undulator parameters as for Fig. 6, field components (*continuous line:* B_y and *dots:* B_x) for the left half of the undulator show the end-field variations after gradually reducing the coil currents for the end segments of *four periods*. It shows a linear increase of the end fields.

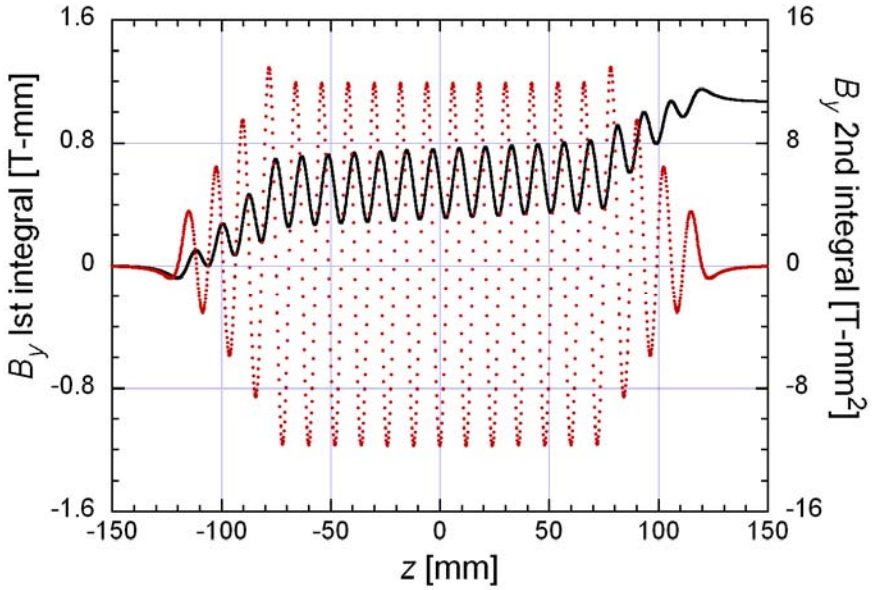

Fig. 9. Field integrals B_y show the effect of end fields. The first integral (*dotted curve*) is almost zero, and the second integral (*continuous line*) is about 10.8 T-mm^2.

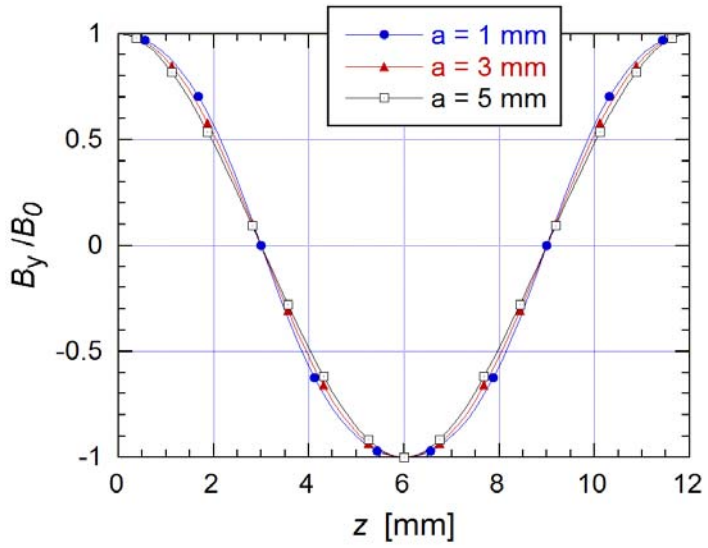

Fig. 10. Normalized vertical fields $B_y(z)/B_0$ were plotted for a planar-type undulator with an engineering current density of 1 kA/mm^2 in the coil. Three values of the coil dimensions in the beam direction were chosen for the calculation.

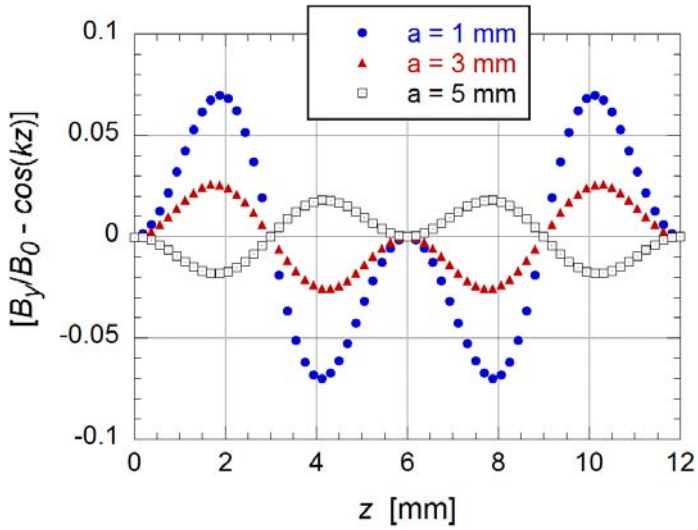

Fig. 11. The residual fields, $B_y(z)/B_0 - cos(kz)$, of Fig. 10 were plotted for a planar-type undulator with the selected three coil dimensions.